LANGMUIR

pubs.acs.org/Langmuir Article

Molecular Basis for the Morphological Transitions of Surfactant Wormlike Micelles Triggered by Encapsulated Nonpolar Molecules

Gervasio Zaldivar, Martin Conda-Sheridan, and Mario Tagliazucchi*

Cite This: *Langmuir* 2021, 37, 3093−3103 Read Online

ACCESS | Metrics & More | Article Recommendations | Supporting Information

ABSTRACT: Surfactant wormlike micelles are prone to experience morphological changes, including the transition to spherical micelles, upon the addition of nonpolar additives. These morphological transitions have profound implications in diverse technological areas, such as the oil and personal-care industries. In this work, additive-induced morphological transitions in wormlike micelles were studied using a molecular theory that predicts the equilibrium morphology and internal molecular organization of the micelles as a function of their composition and the molecular properties of their components. The model successfully captures the transition from wormlike to spherical micelles upon the addition of a nonpolar molecule. Moreover, the predicted effects of the concentration, molecular structure, and degree of hydrophobicity of the nonpolar additive on the wormlike-to-sphere transition are shown to be in good agreement with experimental trends in the literature. The theory predicts that the location of the additive in the micelle (core or hydrophobic−hydrophilic interface) depends on the additive hydrophobicity and content, and the morphology of the micelles. Based on the results of our model, simple molecular mechanisms were proposed to explain the morphological transitions of wormlike micelles upon the addition of nonpolar molecules of different polarities.

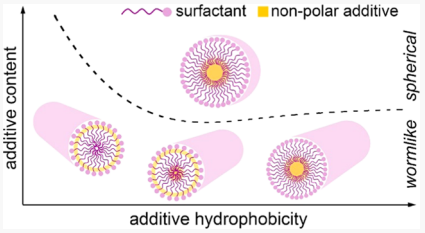

INTRODUCTION

Amphiphilic molecules in solution self-assemble into supramolecular aggregates of different shapes (spheres, cylinders, ribbons, and vesicles, among others). Viscoelastic surfactants (VESs) are a class of amphiphilic molecules that can self-assemble into long wormlike micelles (WM).[1−3] The entanglement of these long cylindrical aggregates imparts interesting rheological properties to the solution, such as high viscosity and elasticity at sufficiently high concentrations.[4] Because of their rheological behavior, VESs find applications as viscosity enhancers in many fields, including personal-care products[5] and fracturing fluids used in oil extraction.[2,6−10] The rheological properties of viscoelastic surfactants in solution remind that of long polymers; however, unlike polymers, wormlike micelles can break and reform under shear.

Applications of VES in personal-care and oil industries usually involve the interaction of wormlike micelles with nonpolar substances, which become incorporated into the micelles. The encapsulation of nonpolar additives can dramatically change the morphology of the aggregates, thereby changing their rheological properties. The most common morphological transition is the transformation of VES wormlike micelles into spherical micelles (SM) (*i.e.*, a wormlike-to-sphere transition) upon the addition of hydrophobic substances.[11−16] In the oil industry, this phenomenon is commonly known as "breaking". In this industry, VESs are used as viscosity enhancers to facilitate the transportation of proppants to the fracture sites. There, the wormlike micelles in contact with the hydrocarbons break into spherical aggregates,[10,17] which greatly decreases the viscosity of the fluid and facilitates its removal. This process implies a major advantage of VES over polymeric viscosity enhancers[9,10] that are difficult to remove from the reservoirs.

The mechanism by which the incorporation of small nonpolar molecules into wormlike micelles affects their morphology is not only a highly relevant technological issue but also a fascinating fundamental problem. This transition has been proposed to occur by the dissolution of nonpolar guests into the core of the wormlike micelles, which was proposed to increase their curvature up to the point where spherical micelles become more favorable than cylinders.[12] However, oil dissolution into the cylinder core should increase its diameter and, therefore, reduce (rather than increase) the interfacial curvature.[11] Recent experimental studies have revealed complex mechanisms of hydrocarbon-induced wormlike-to-sphere transition. For example, when the hydrocarbon is an aromatic alkane (*e.g.*, benzene, toluene, or ethylbenzene), the length of the wormlike micelles first increases and then decreases with increasing hydrocarbon content.[14,15,18] To explain the unusual behavior of aromatic hydrocarbons, it has been proposed that these molecules dissolve close to the hydrophobic−hydrophilic interface (outer palisade re-

Received: November 29, 2020
Revised: February 17, 2021
Published: March 8, 2021

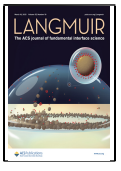

https://dx.doi.org/10.1021/acs.langmuir.0c03421
Langmuir 2021, 37, 3093−3103

gion),[14,15,18] while aliphatic species preferentially dissolve into the nonpolar core. Taken together, these observations show that the mechanisms of disassembly of wormlike micelles induced by small nonpolar molecules are complex and still poorly understood.

Both the formation of wormlike micelles and how they are affected by nonpolar additives have been studied by molecular dynamics (MD) simulations[19−25] and theoretical tools[26−31] in the past. MD simulations provide structural information about the aggregates; however, their use in systematic studies is greatly hampered by the time and length scales involved in micellar aggregation. Moreover, estimating the thermodynamic stability (free energy) of different types of micellar structures using MD simulations would be computationally very costly. On the other hand, classical analytical theories provide an estimation of the thermodynamic stability of the different potential morphologies of the system, but these theories provide limited structural information. Moreover, simple theories do not consider the chemical structures of the surfactant and oil molecules in detail, which seem to be critical to fully understand the morphological behavior of these sytems.[14,15,18,32,33]

We present here a theoretical approach designed to study the co-aggregation of surfactants and small molecules in water−salt solutions, using a thermodynamical statistical tool known as molecular theory (MOLT).[34−38] This approach provides both detailed structural and thermodynamic information of the system while explicitly considering the molecular details of the surfactant and additives at a coarse-grain level of description. The economical computational cost of the MOLT allows us to systematically explore different conditions. In this work, we applied this tool to model co-aggregates formed by a surfactant whose properties resemble the properties of cetyltrimethylammonium bromide (CTAB) and a linear nonpolar molecule of variable hydrophobicity and length. Our predictions of the morphology diagram of the aggregates as a function of the hydrophobicity of the nonpolar additive and its content are in good agreement with experimental observations in the literature. Based on the results of our model, we propose simple mechanisms that explain the behavior of wormlike micelles in the presence of additives of different polarities and at various concentrations. Our results provide a theoretically grounded molecular basis for some of the tentative mechanisms put forward in the literature.[10,11,14,15,18]

THEORETICAL METHODS

General Model. Our theory is based on our previous studies on the self-assembly of neutral triblock surfactants[37] and lysine-terminated peptide amphiphiles.[38] It is derived from a MOLT previously developed by Szleifer and co-workers.[34−36] The theory explicitly takes into account the molecular details of the surfactant and nonpolar molecules (*i.e.*, their chemical structures, conformations, volume and charge distributions, inter and intramolecular interactions) and the properties of the solution (ionic strength and pH). The theory is formulated in detail in the Supporting Information and briefly discussed here.

The model system consists of a co-assembly of N_S surfactant and N_{NP} nonpolar molecules in a volume V at temperature T. The aggregate is fixed in space (*i.e.*, our theory provides a stability criterion for isolated aggregates, and it does not include the translational degrees of freedom of the aggregate; see below), and it is in contact with an aqueous NaCl bulk solution. We used a coarse-grain model for the surfactant and nonpolar molecules. Each coarse-grain bead in our model represents four heavy (non-H) atoms. The chemical structure of the surfactant was chosen to specifically model cetyltrimethylammonium bromide (CTAB), which exhibits high propensity to form wormlike micelles.[13,39,40] The CTAB molecules were modeled using two types of beads, *i.e.*, alkyl-tail beads that represent four methylene groups (colored dark purple in Figure 1)

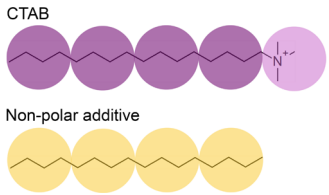

Figure 1. Top: mapping between the chemical structure and the coarse-grain model for CTAB. Bottom: the nonpolar molecule used in this work is a linear chain of coarse-grained beads and variable hydrophobicities. For example, if each bead has the same properties as the tail beads of the CTAB molecule, then a four-bead molecule corresponds to a model of *n*-hexadecane.

and head beads that stand for the quaternary ammonium functionality (colored light purple in Figure 1). Nonpolar molecules were generically modeled as a linear chain of coarse-grained beads of varying hydrophobicities and numbers (colored yellow in Figure 1). In the specific case where the beads of the nonpolar molecule have the same properties as the CTAB-tail beads, our coarse-grain nonpolar molecule models a linear alkane, where each bead represents four methylene units. However, we kept the hydrophobicity of the beads of the nonpolar additive as a tunable parameter in our model to explore its effect on the wormlike-to-sphere transition (see Introduction).

The mobile salt ions have a constant chemical potential fixed by the composition of the bulk solution. The thermodynamical potential that minimizes at equilibrium is a semigrand canonical potential $\Omega^*(T, V, N_S, N_{NP}, \{\mu_i\})$, where N_S and N_{NP} are the total number of surfactant and nonpolar molecules, respectively, and $\{\mu_i\}$ is the chemical potential of the salt ions (i = cation or anion). The * superscript indicates that Ω^* describes an aggregate fixed in space, so it lacks translational and rotational entropy (resembling Israelachvili's model for the chemical potential of surfactants in a fixed aggregate[41]). Note that the functional Ω^* is canonical for the surfactant and the nonpolar molecule but grand canonical for the ions and the solvent.

We wrote down an approximate expression for Ω^* as a functional of structural functions of the system that are *a priori* unknown. These functions are the local number density of the different species in the system, $\rho_i(\mathbf{r})$ (i = surfactant, nonpolar molecule, solvent, salt anion, and cation), the position-dependent probability distribution functions for the conformations of the surfactant and nonpolar molecules, $P_k(\alpha,\mathbf{r})$ (k = surfactant or nonpolar molecule), and the local electrostatic potential, $\psi(\mathbf{r})$. For the sake of generality, in the following description of the theory, we will assume that these structural functions can depend on $\mathbf{r}$, *i.e.*, the (x,y,z) position in the system. Note, however, that in this work we took advantage of the symmetry of the systems under study, which allowed us to consider inhomogeneities only in one dimension at the moment of solving the theory (see Section 2 and Supporting Information (SI)).

The proposed expression for Ω^* (which we will hereafter refer to as the free energy of the system for simplicity) is

https://dx.doi.org/10.1021/acs.langmuir.0c03421
Langmuir 2021, 37, 3093−3103

$$\beta\Omega^* = \beta F^* - \sum_{\substack{i=\text{anion,}\\ \text{cation}} } N_i\beta\mu_i = \sum_{\substack{i=\text{S,NP,anion,}\\ \text{cation,sol}}} \int \rho_i(\mathbf{r})[\ln(\rho_i(\mathbf{r})\nu_{\text{sol}}) - 1]\, d\mathbf{r}$$
$$+ \sum_{k=\text{S,NP}} \int \rho_k(\mathbf{r}) \sum_{\alpha} P_k(\alpha, \mathbf{r})\ln(P_k(\alpha, \mathbf{r}))\, d\mathbf{r}$$
$$-\frac{1}{2} \sum_{\substack{i=\text{all bead}\\ \text{types}}} \sum_{\substack{j=\text{all bead}\\ \text{types}}} \int\int \langle n_i(\mathbf{r})\rangle\langle n_j(\mathbf{r}')\rangle\beta \in_{ij} g_{ij}(\mathbf{r}, \mathbf{r}')\, d\mathbf{r}\, d\mathbf{r}'$$
$$+\beta \int \left[\langle \rho_Q(\mathbf{r})\rangle\psi(\mathbf{r}) - \frac{\varepsilon(\mathbf{r})}{2}[\nabla\psi(\mathbf{r})]^2\right] d\mathbf{r} - \sum_{\substack{i=\text{anion,}\\ \text{cation}}} \beta\mu_i \int \rho_i(\mathbf{r})\, d\mathbf{r} \quad (1)$$

where $\beta = (k_BT)^{-1}$, ν_{sol} is the volume of solvent molecules, $\langle n_i(\mathbf{r})\rangle$ is the average number density of beads of type i at position $\mathbf{r}$, ϵ_{ij} is the parameter that controls the strength of the interactions between beads of type i and j, $g_{ij}(\mathbf{r},\mathbf{r}')$ is a function that dictates the spatial dependence of that interaction, $\langle \rho_Q(\mathbf{r})\rangle$ is the average charge density at position $\mathbf{r}$, and $\varepsilon(\mathbf{r})$ is the position-dependent dielectric permittivity. The first term on the right-hand side of eq 1 accounts for the free energy associated with the translational entropy (which is related to the mixing entropy) of all species in the system (surfactant, nonpolar molecule, solvent, and ions). The second term is the free energy related to the conformational entropy of surfactant and nonpolar molecules. In this term, the sum over α includes, in principle, the set of all possible conformations for each of these molecules, but in practice it is enough to consider a representative subset. The third term is the energy of the effective short-range attractive interactions between all types of beads (*i.e.*, the sums run over all types of beads of the nonpolar additive and the surfactant). The fourth term is the electrostatic contribution to the free energy. Finally, the last term accounts for the $-N\mu$ terms for the cation and the anion, which have a fixed chemical potential and should be included in Ω^* because this functional is grand canonical for these two species. For a full description of each contribution to Ω^*, we refer the reader to the Supporting Information (SI).

We obtain the equilibrium morphology and structural properties of the system by finding the extrema of Ω^* with respect to $\psi(\mathbf{r})$, $P_k(\alpha,\mathbf{r})$ (k = surfactant or nonpolar molecule), and $\rho_i(\mathbf{r})$ (i = surfactant, nonpolar molecule, solvent, cation, and anion) subjected to the following restrictions:

(i) The packing or incompressibility constraint. The sum of the volume fractions of all species at each position should be 1. This restriction models intermolecular repulsive interactions in the system as excluded-volume interactions.
(ii) The global electroneutrality constraint. The net charge in the whole volume of the system is zero (note that electroneutrality is imposed globally, not locally).
(iii) The normalization of the functions $P_k(\alpha,\mathbf{r})$ for k = surfactant or nonpolar molecule at each $\mathbf{r}$.
(iv) Constraints enforcing that the integrals of $\rho_k(\mathbf{r})$, for k = surfactant or nonpolar molecule, in the whole volume of the system should be equal to N_S and N_{NP}, respectively.

The extremization of Ω^* subjected to restrictions (i)−(iv) leads to explicit expressions for the unknown structural functions mentioned above. These expressions compose a set of coupled integrodifferential equations that is discretized and numerically solved. The code developed by us to solve the theory is available upon request.

The inputs of the theory include the chemical structure of the nonpolar and surfactant molecules, a representative set of their conformations, the salt concentration of the solution, the strength of the short-range effective attractions between the different types of beads, and the electric charge and molecular volume of those beads. The representative set of conformations of the surfactant and nonpolar molecules was randomly generated using a rotationally isomeric state (RIS) model[42,43] (see Section S1d.ii in the Supporting Information). Each conformation defines both the internal degrees of freedom (dihedral angles in the RIS model) and the orientation of the molecule in three dimensions. We generated 10^4 conformations for each type of molecule (surfactant or nonpolar molecules) and each possible position of the molecular center of mass. The size of this set is large enough to ensure that all of the thermodynamic and structural properties of the system are converged; see SI of ref 38.

The strengths of the attractive interactions between the different types of coarse-grain beads were adapted from the Martini MD coarse-grain force field[44,45] using the procedure reported in our previous work[38] (see the Supporting Information). Table S1 (Supporting Information) reports the parameters that govern those interactions, ϵ_{ij} (where i and j represent types of beads). For example, the self-interaction of surfactant-tail beads is $\epsilon_{T-T} = 7.0\ k_BT$. To scan the hydrophobicity of the nonpolar molecule, we manually constructed a hydrophobicity scale by setting the strength of the interactions between nonpolar beads, ϵ_{NP-NP}, to a value between 7.0 k_BT (highly hydrophobic) and 3.0 k_BT (poorly hydrophobic) and then calculating the strength of the cross interactions ϵ_{NP-T} as a geometric average between ϵ_{T-T} and ϵ_{NP-NP} (see SI for further details). This approach has the advantage of allowing to continuously tune the hydrophobicity of the guest molecule without changing its other properties, thereby allowing to isolate the effects of hydrophobicity. However, our strategy conceals how the nonpolar molecules in our model are related to specific chemical structures. In Section 1 of the results, we show how selected points in our scale are related to Martini bead types, which enables us to assign examples of specific chemical structures to the nonpolar molecules of different hydrophobicities in our model.

The theory provides thermodynamic and structural information on the system, such as its free energy Ω^*; the local number density of the species, $\rho_i(\mathbf{r})$; the probability distribution function of the conformations of the surfactant and additive, $P_k(\alpha,\mathbf{r})$; and the local electric potential, $\psi(\mathbf{r})$.

Morphology of the Aggregates and Thermodynamic Stability. As in our previous studies,[37,38] we assessed the morphology of the aggregates by considering three possible ideal shapes: spheres, infinitely long cylinders (wormlike micelles), and infinitely extended planar lamellas. These three ideal morphologies can be described using only one spatial coordinate, r, which represents the radial distance for spheres and cylinders and the distance to the central plane for lamellas. In this approach, heterogeneities are allowed only in the r direction and the system is assumed to be homogeneous in the other two directions. The derivation of the theory upon this assumption is straightforward (see SI and refs 37, 38). This approximation significantly diminishes the complexity and computational cost of the calculations, which permits a systematic exploration of the morphology diagram.

To compare the stability of the different morphologies, we calculated the free energy per molecule in excess to the bulk solution defined by

$$\omega^{*,\text{ex}}(T, N_S, N_{NP}, \{\mu_i\}) = \frac{\Omega^{*,\text{ex}}(T, N_S, N_{NP}, \{\mu_i\})}{N_S + N_{NP}}$$
$$= \frac{\Omega^*(T, V, N_S, N_{NP}, \{\mu_i\}) - \Omega^*(T, V, N_S = 0, N_{NP} = 0, \{\mu_i\})}{N_S + N_{NP}} \quad (2)$$

where $\{\mu_i\} = \mu_{\text{anions}}, \mu_{\text{cations}}$. The first equality states that $\omega^{*,\text{ex}}$ is a free energy per molecule, and the second equality indicates that $\omega^{*,\text{ex}}$ and $\Omega^{*,\text{ex}}$ are, respectively, differences between the corresponding quantities in the system of interest and in a system having the same volume and chemical potential of the ions as the system of interest but lacking surfactants and additives. In the last term of eq 2, $\Omega^*(T, V, N_S = 0, N_{NP} = 0, \{\mu_i\})$ is the (semigrand canonical) free energy of the latter system, *i.e.*, a system without aggregates at fixed volume V. Note that the superscript "ex" in $\omega^{*,\text{ex}}$ and $\Omega^{*,\text{ex}}$ indicates, therefore, the difference of a quantity in the system of interest and the bulk and it does not convey the common meaning of a thermodynamic excess quantity (the difference between a quantity and its value in an ideal

https://dx.doi.org/10.1021/acs.langmuir.0c03421
Langmuir 2021, 37, 3093−3103

reference state). As we previously demonstrated,[38] $\omega^{*,ex}$ is independent of the volume of the system and it is the proper thermodynamic potential to compare the stability of systems with a different number of molecules and morphologies.

In practice, we solve the theory for a given set of conditions, which include the solution salt concentration, the hydrophobicity of the nonpolar additive (given by ϵ_{NP-NP}), and its mole fraction, $x_{NP} = N_{NP}/(N_{NP} + N_S)$. We calculate $\omega^{*,ex}$ for aggregates with the three possible ideal morphologies and different aggregation numbers (molecules per spherical micelle) or densities (molecules per unit length of cylindrical wormlike micelles, or molecules per unit area of lamellar micelles). The aggregate (defined by its morphology and aggregation number or density) with the lowest value of $\omega^{*,ex}$ represents the equilibrium state of the system. We should mention that for the system and conditions discussed in this work, the lamella morphology was always less stable than that of the micelles and/or the fibers and, therefore, it is not discussed hereafter.

RESULTS

Transition from Wormlike to Spherical Micelles with the Increasing Content of the Nonpolar Additive. Figure 2a shows the morphology diagram of co-aggregates formed by CTAB and a nonpolar additive of four coarse-grain beads (each one representing approximately four non-H atoms) as a function of the strength of the interaction between the beads of the nonpolar molecule given by the parameter ϵ_{NP-NP} (values from 3.0 to 7.0 k_BT were explored) and its mole fraction in the aggregate, x_{NP}. Larger values of ϵ_{NP-NP} correspond to a more hydrophobic additive. The largest considered value, ϵ_{NP-NP} = 7.0 k_BT, corresponds to alkane-like hydrophobicity, *i.e.*, the four-bead additive with ϵ_{NP-NP} = 7.0 k_BT is a model of *n*-hexadecane, according to our parametrization based on the Martini model;[44] see Theoretical Methods section and SI. For ϵ_{NP-NP} = 4.8 k_BT, the MOLT bead approximately corresponds to a C4 Martini bead. The C4 Martini bead is used to model, for example, a linear chain of four carbon atoms with two unsaturations, so a nonpolar molecule with ϵ_{NP-NP} = 4.8 k_BT will be a model of a polyunsaturated alkene.[44] A MOLT bead with ϵ_{NP-NP} = 3.5 k_BT (close to the lowest end of our hydrophobicity scale) approximately corresponds to a C5 Martini bead, which, for example, is used to describe a chain of three carbon atoms and one sulfur atom (*i.e.*, an alkyl sulfide).[44] Both C4 and C5 beads differ from MOLT beads in the cross interaction ϵ_{T-NP}, but the difference is small to qualitatively influence the results. Finally, comparison with a recent Martini model of poly(ethylene oxide) (PEO) indicates that a PEO chain is less hydrophobic than a nonpolar molecule with ϵ_{NP-NP} = 3.5 k_BT.[46]

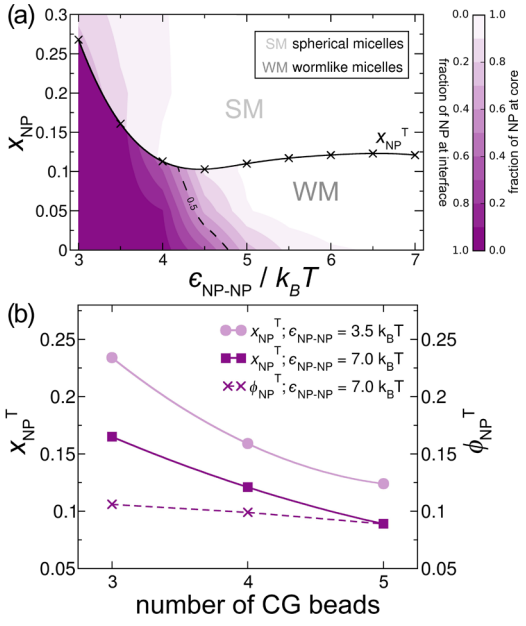

Figure 2. (a) Colormap of the fraction of the nonpolar additive at the interface between the hydrophobic and hydrophilic regions of the micelle as a function of the mole fraction of additive, x_{NP}, and the strength of the interaction between two beads of the nonpolar molecule, ϵ_{NP-NP}. The dashed line indicates the boundary where half of the additive is located at the core and the other half at the hydrophobic−hydrophilic interface. The solid black line is the mole fraction of the additive at the wormlike-to-sphere transition as a function of ϵ_{NP-NP} (tagged as x_{NP}^T), which demarks the zones of stability of the spherical (SM) and wormlike (WM) micelles. The additive is composed of four coarse-grain beads. (b) Mole fraction (solid lines, x_{NP}^T) and total volume fraction (dashed line, ϕ_{NP}^T) of the nonpolar additive at the wormlike-to-sphere transition as a function of the number of the coarse-grain beads forming the nonpolar additive. x_{NP}^T is shown for ϵ_{NP-NP} = 3.5 and 7.0 k_BT, while ϕ_{NP}^T is shown for ϵ_{NP-NP} = 7.0 k_BT. In all plots, the salt concentration was fixed to 0.1 M.

In the absence of the additive (x_{NP} = 0), Figure 2a shows that the surfactant forms cylindrical (wormlike) micelles. Upon an increase in the content of the nonpolar guest, the aggregates experience a transition from wormlike to spherical micelles for all values of ϵ_{NP-NP}. This transition has been experimentally observed in many surfactant/hydrocarbon/salt/water systems.[11,12,14,15,17] In particular, Hoffmann et al.[13] showed that a water solution with equimolar concentrations of CTAB and sodium salicylate experiences a transition from rodlike to spherical micelles following the addition of alkanes of different lengths. For *n*-tetradecane (the longest hydrocarbon studied), the transition occurred at an alkane mole fraction of 0.1, in good agreement with our results for ϵ_{NP-NP} = 7.0 k_BT (alkane-like hydrophobicity) in Figure 2a. Furthermore, Shibaev et al.[11] observed the same transition for an anionic surfactant (potassium oleate) in a KCl−water solution at a ∼0.2 mol fraction of *n*-dodecane, which is also qualitatively consistent with our predictions. Note that some degree of quantitative disagreement between experiments and theory is expected due to the differences between our model and the experimental systems, the approximations involved in our theory, and the experimental uncertainties associated with detecting morphological transitions throughout indirect measurements, such as rheological properties,[11,14] light scattering,[12,13] or model-dependent determinations.[14,15]

Increasing the number of coarse-grain beads in the additive molecule leads to a decrease in the mole fraction at the wormlike-to-sphere transition, x_{NP}^T; see Figure 2b. This result is in good agreement with the report of Hoffmann et al.,[13] who observed exactly the same trend for the CTAB−salicylate−alkane system.

Influence of the Hydrophobicity of the Nonpolar Additive. Figure 2a shows that as the hydrophobicity of the additive decreases, its mole fraction at the transition, x_{NP}^T, changes nonmonotonically and displays a minimum at ϵ_{NP-NP} = 4.5 k_BT. For mildly hydrophobic additives (ϵ_{NP-NP} < 4.5 k_BT), the mole fraction at the wormlike-to-sphere transition increases with decreasing hydrophobicity, while for highly hydrophobic additives (ϵ_{NP-NP} > 4.5 k_BT), it slightly increases with increasing hydrophobicity and reaches a plateau. The

https://dx.doi.org/10.1021/acs.langmuir.0c03421
Langmuir 2021, 37, 3093−3103

increase in x_{NP}^{T} with decreasing hydrophobicity is in qualitative agreement with experimental data.[13,15,16] For example, Hoffmann et al.[13] observed that a tetradecyltrimethylammonium bromide (TTABr) aqueous solution experiences a transition from rodlike to globular micelles at ∼0.2 mol fraction of *n*-decane, while the same transition occurs at a ∼0.33 mol fraction of butylbenzene. Furthermore, a betaine-based surfactant was shown to experience the wormlike-to-sphere transition at ∼0.5 mol fraction for methylcyclohexane and *n*-heptane, but for toluene, the transition mole fraction increases to ∼0.75.[16] In both examples, the species being compared have the same number of atoms and, therefore, similar molecular volume, but the aromatic molecules are less hydrophobic than the aliphatic ones (*i.e.*, as estimated from their respective octanol/water partition coefficients[47]).

As we explain in detail below, the influence of the hydrophobicity of the additive on the wormlike-to-sphere transition is related to the distribution of the nonpolar molecules within the aggregates. The guest can be located either at the core of the aggregate or at the interface between the hydrophobic and the hydrophilic regions of the micelles (the outer part of the palisade region). Figure 3 shows the volume fraction of the additive, the surfactant-tail, and the surfactant-headgroup segments as a function of the distance to the central axis of a wormlike micelle. Depending on the hydrophobicity of the additive, it can be localized either at the micellar core (ϵ_{NP-NP} = 7.0 k_BT, Figure 3a) or at the hydrophobic−hydrophilic interface (ϵ_{NP-NP} = 3.0 k_BT, Figure 3b). We should mention the existence of intermediate structures, where a fraction of molecules is located at the center and the rest at the interface.

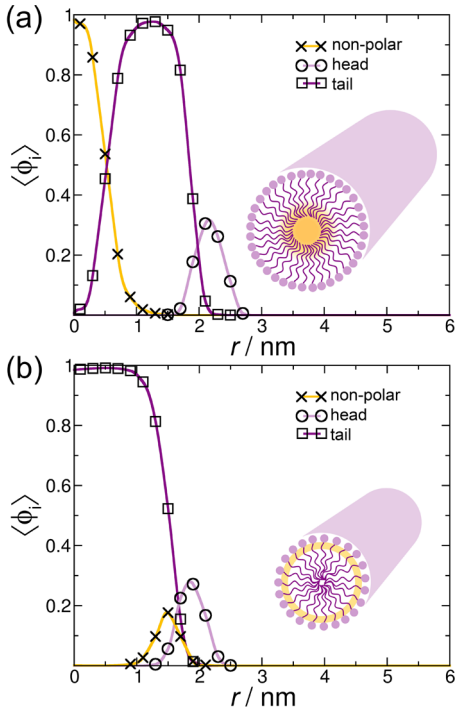

Figure 3. Volume fraction of beads of type *i*, $\langle\phi_i\rangle$ (*i* = nonpolar molecule, surfactant-tail, or surfactant-headgroup beads) as a function of the distance to the central axis of a cylindrical wormlike micelle for ϵ_{NP-NP} = 7.0 k_BT (a) and 3.0 k_BT (b). The insets show schematic drawings of a transversal cut of the micelles, stressing the distribution of the constitutive parts of the aggregates. The salt concentration was fixed at 0.1 M.

We determined the fraction of nonpolar molecules at the micellar core and hydrophobic−hydrophilic interface (outer palisade region) by (arbitrarily) defining a cutoff position at the maximum of the volume fraction of tail beads (see dark purple lines with squares in Figure 3). Beads located between the center of the structure (r = 0) and this cutoff position are assigned to the core, while the remaining beads are assigned to the palisade region. The colormap in Figure 2a shows the fraction of nonpolar molecules at the hydrophobic−hydrophilic interface as a function of x_{NP} and ϵ_{NP-NP}. Purple regions indicate structures where the nonpolar molecule is mainly located at the palisade region. Note that in spherical aggregates, nonpolar molecules are predicted to be mainly located at the core for all values of ϵ_{NP-NP}. Conversely, in wormlike micelles, nonpolar additives are located at the palisade region if their hydrophobicity and mole fraction are low and at the micellar core otherwise. The boundary between both regimes (at which the guest molecule is equally distributed between the core and the hydrophobic−hydrophilic interface; see the dashed line in Figure 2a) coincides with the minimum of the x_{NP}^{T} *vs* ϵ_{NP-NP} curve at ϵ_{NP-NP} = 4.5 k_BT. This result suggests that the location of the nonpolar guest molecules is key to understanding the influence of the additive on the morphology of the aggregates. This issue will be addressed in detail below, where we independently analyze the two regimes shown in Figure 2 defined by the hydrophobicity of the nonpolar molecule.

Highly Hydrophobic Nonpolar Additives (ϵ_{NP-NP} > 4.5 k_BT). In this regime, almost all nonpolar molecules are located at the core of the aggregate (see the colormap in Figure 2a). In this case, the number of guest molecules within an aggregate roughly dictates its size: the volume of spherical and wormlike micelles increases with the mole fraction of the nonpolar molecule (see Figure S2 in the Supporting Information). The change in size and surface curvature allows for a simple explanation of the wormlike-to-sphere transition in the context of Israelachvili's packing theory.[41] This theory explains the shape of micellar aggregates in terms of the "shape" of the surfactant molecules that compose them. Briefly, conical-like molecules promote curved aggregates (*e.g.*, micelles). As the shape of the molecule evolves from conical-like to cylinder-like, the aggregate undergoes micelle → fiber → lamella transitions. Note that the packing theory is mainly qualitative because the "shape" of a molecule is not a well-defined concept. The MOLT used in this work does not depend on this concept, although its predictions agree in general very well with those of the packing theory.[37]

Figure 4a shows the mean curvature of spherical and wormlike micelles as a function of the mole fraction of the additive, x_{NP}. Note that this plot considers the properties of both morphologies, despite the fact that only one of them is the equilibrium structure (global free-energy minimum) for a given value of x_{NP} (the other structure is a local free-energy minimum). We have already shown that in the absence of guest molecules (x_{NP} = 0), wormlike micelles are more stable than spherical ones (Figure 2a). Therefore, the mean curvature of the wormlike cylindrical micelles in the absence of nonpolar guests (H = 0.3 nm^{-1}, see Figure 4a) should be close to the optimal curvature for the surfactant, which, according to Israelachvili's packing theory, depends on its "shape". On the other hand, the curvature of spherical micelles (H = 0.44

https://dx.doi.org/10.1021/acs.langmuir.0c03421
Langmuir 2021, 37, 3093−3103

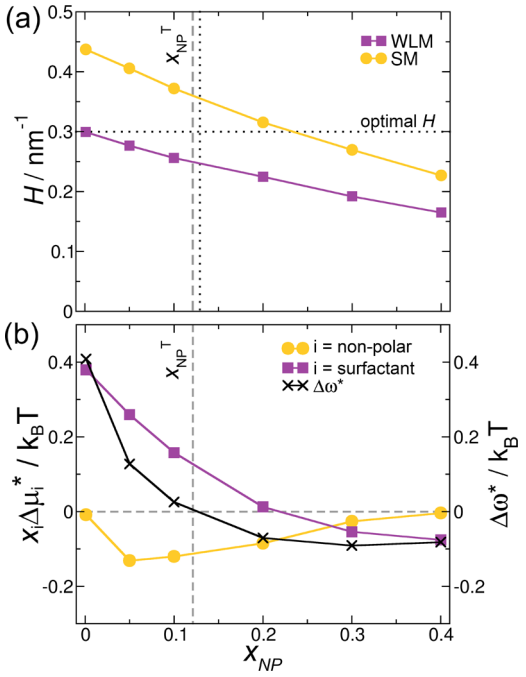

Figure 4. (a) Mean curvature of spherical (yellow circles) and wormlike (purple squares) micelles as a function of the mole fraction of the nonpolar molecule, x_{NP}, for co-aggregates formed by CTAB and a four-bead nonpolar molecule. The horizontal dotted line indicates the estimated optimal curvature for the surfactant. The vertical dotted line marks the fraction of the nonpolar additive at which the curvatures of spherical and cylindrical are equally distant from the optimal curvature. (b) Change in the free energy per molecule ($\Delta\omega^*$) and the chemical potential of species i (μ_i^*, i = surfactant, nonpolar molecule) multiplied by x_i for the transformation of wormlike to spherical micelle as a function of x_{NP}. In (a) and (b), the vertical gray dashed line marks the x_{NP} at the wormlike-to-sphere transition (x_{NP}^T). Salt concentration was fixed to 0.1 M and ϵ_{NP-NP} to 7.0 k_BT.

nm^{-1}) is expected to be larger than the optimal curvature. As x_{NP} increases, so does the radius of both the spherical and the wormlike micelles, causing a decrease in their mean curvatures (see Figure 4a). This behavior implies that the curvature of the cylindrical micelle starts to deviate from the optimal value ($H \sim 0.3$ nm^{-1}, marked with a horizontal dotted line in Figure 4a), while that of the spherical micelles gets progressively closer to it. Therefore, from the packing-theory point of view, the wormlike-to-sphere transition should approximately take place when the curvature of the micelle is closer to the optimal value of $H \sim 0.3$ nm^{-1} than that of the cylinder. This condition occurs for $x_{NP} = 0.129$ (the vertical black dotted line in Figure 4a), which is in fact very similar to the transition fraction determined from the free energy of the aggregates, $x_{NP}^T = 0.121$ (the vertical gray dashed line in Figure 4a). The proposed mechanism is schematized in Figure 6a.

To provide further support for the argument that the change of aggregate curvature triggers the wormlike-to-sphere transition, we looked at the thermodynamics of the system. Let us consider the contributions to the free energy per molecule

$$\omega^* = \frac{\Omega^*}{N_S + N_{NP}} = \frac{F^*}{N_S + N_{NP}} - \sum_{i=\text{anion,cation}} \frac{\mu_i N_i}{N_S + N_{NP}}$$
$$= \mu_S^* x_S + \mu_{NP}^* x_{NP} - \frac{pV}{N_S + N_{NP}} \quad (3)$$

where in the first equality, we used the definition of ω^*, *i.e.*, ω^* is the semigrand canonical free energy per molecule and, therefore, it is equal to Ω^* (the semigrand canonical free energy) divided by the total number of surfactant + additive molecules. In the second equality of eq 3, we used the definition of the semigrand canonical potential, $\Omega^* = F^* - \sum_{i=\text{anions,cations}} \mu_i N_i$, where i runs over those species whose chemical potential is fixed (*i.e.*, the anions and cations). In the third equality, we used the definition of the Helmholtz free energy, $F^* = \sum_{i=\text{anions,cations}} \mu_i N_i + \sum_{j=S,NP} \mu_j^* N_j - pV$, and $x_i = N_i/(N_S + N_{NP})$ for i = S (surfactant) or NP (nonpolar molecule). Note that we use the "*" superscript (which indicates that the thermodynamic quantity corresponds to an aggregate fixed in the space) for the chemical potentials of the surfactant and the additive but not for those of the anions and cations, which are fixed by the bulk solution.

We will focus our attention on the $x_S\mu_S^*$ and $x_{NP}\mu_{NP}^*$ terms on the right-hand side of eq 3. Let us define $x_i\Delta\mu_i^*$ as the change in each of those terms for a wormlike-to-sphere transition at fixed composition, *i.e.*, $x_i\Delta\mu_i^* = x_i(\mu_i^{*,\text{sphere}} - \mu_i^{*,\text{wormlike}})$. When $x_i\Delta\mu_i^*$ is negative, molecules of type i would prefer to be in a spherical aggregate rather than in a wormlike micelle, and *vice versa* for $x_i\Delta\mu_i^* > 0$. Figure 4b shows $x_i\Delta\mu_i^*$ and the total free-energy difference ($\Delta\omega^* = \omega^{*,\text{sphere}} - \omega^{*,\text{wormlike}}$) as a function of x_{NP}. Note that $\Delta\omega^* \cong x_S\Delta\mu_S^* + x_{NP}\Delta\mu_{NP}^*$; thus, the contribution of the $pV/(N_S + N_{NP})$ term in eq 3 to the following analysis is negligible. As x_{NP} increases, the surfactant contribution (purple line) decreases up to the point at which it becomes negative. This behavior remarkably suits the mechanism proposed above from packing arguments: as the curvature of both types of aggregates decreases, the surfactant increasingly prefers the spherical environment. In contrast, the contribution of the nonpolar molecules always favors spherical micelles ($x_i\Delta\mu_i^* < 0$ for i = nonpolar molecule), probably because the spherical shape minimizes the interfacial tension at the hydrophilic–hydrophobic interface. Moreover, the $x_{NP}\Delta\mu_{NP}^*$ contribution changes only slightly with x_{NP}. In sum, this result supports the idea that the key factor dictating the transition from wormlike to spherical micelles triggered by highly hydrophobic additives is the change in the curvature of the aggregates and its effect on the chemical potential of surfactant molecules.

Remarkably, the proposed mechanism explains two results shown in Figure 2. Namely

(1) The mole fraction of the nonpolar molecule at the wormlike-to-sphere transition shows a plateau at high hydrophobicities (see Figure 2a). This trend is explained by the fact that, in this regime, the transition depends only on the volume occupied by the additive at the core of the aggregate. Therefore, as long as the hydrophobicity of the additive is high enough to ensure that it resides at the core of the wormlike micelle ($\epsilon_{NP-NP} > 4.5$ k_BT), the transition becomes independent of ϵ_{NP-NP}.

(2) The mole fraction of the additive at the transition decreases with the increase of the number of beads in its

https://dx.doi.org/10.1021/acs.langmuir.0c03421
Langmuir 2021, 37, 3093−3103

structure (see Figure 2b). Once again, this effect results from the fact that the main parameter triggering the transition is the volume that the guest molecule occupies at the core of the aggregate. Therefore, the transition occurs at a lower mole fraction for long bulky molecules than for short small ones. To further support this conclusion, we plotted the total volume fraction of nonpolar molecules at the transition, $\phi_{NP}^{T} = V_{NP}/(V_{NP} + V_S)$ (where V_i is the volume occupied by surfactant (i = S) or additive (i = NP) molecules within the aggregate), as a function of the number of coarse-grain beads composing the additive; see Figure 2b. The figure shows that the transition occurs roughly at the same additive volume fraction.

At this point, we must say that the mechanism proposed above is an attempt to provide a simple rationalization of a rather complex, multivariable process. The morphology of aggregates depends on the subtle competition between all of the contributions to the free energy. We advise the reader against straightforwardly extending our conclusions to other systems without a prior examination of how the specific molecular details of the system may affect the relative importance of the contributions discussed above.

Mildly Hydrophobic Nonpolar Additives (ϵ_{NP-NP} < 4.5 k_BT). Nonpolar additives at low mole fractions (x_{NP} < 0.25) and of low hydrophobicity are located at the hydrophobic−hydrophilic interface of the wormlike micelles, as shown in Figure 5a. As a consequence, in this regime, wormlike micelles do not grow in size or change their curvature with increasing x_{NP}; see Figures S2 and 5b, and the scheme in Figure 6b. Moreover, for mildly hydrophobic additives, the change in chemical potential for the wormlike-to-sphere transformation, $x_i\Delta\mu_i^*$ (see Figure 5c), has a different behavior to that observed in Figure 4b for highly hydrophobic additives. In the present case, $x_i\Delta\mu_i^*$ shows two regions: (1) For x_{NP} < 0.25, the contribution of the chemical potential of surfactant molecules, $x_S\mu_S^*$, is lower in wormlike micelles than in spherical micelles ($x_S\Delta\mu_S^*$ > 0) and that of nonpolar molecules, $x_{NP}\mu_{NP}^*$, is lower in spherical micelles than in wormlike micelles ($x_{NP}\Delta\mu_{NP}^*$ < 0). Notably, as the content of nonpolar molecules increases, $x_{NP}\Delta\mu_{NP}^*$ progressively decreases, *i.e.*, they increasingly favor the spherical micelles. (2) For x_{NP} > 0.25, the behavior is similar to that of highly hydrophobic nonpolar molecules reported in Figure 4a, *i.e.*, the surfactant increasingly stabilizes within the spherical micelle, while the contribution from the chemical potential of the additive shows only a small change, which is expected because in these conditions the nonpolar guest is located at the core for both morphologies.

The behavior of the system at high additive content (x_{NP} > 0.25) is the same for highly and mildly hydrophobic additives, *i.e.*, in both cases, spherical micelles are stabilized with respect to cylindrical ones because of the surfactant chemical potential. However, the wormlike-to-sphere transition for mildly hydrophobic additives (which occurs at $x_{NP}^{T} \sim 0.161$ for ϵ_{NP-NP} = 3.5 k_BT) shows two important differences compared to that predicted for highly hydrophobic additives: (i) It occurs at a higher additive mole fraction ($x_{NP}^{T} \sim 0.161$ for ϵ_{NP-NP} = 3.5 k_BT) than for highly hydrophobic guest molecules ($x_{NP}^{T} \sim 0.121$ for ϵ_{NP-NP} = 7.0 k_BT). (ii) The driving force is different. For highly hydrophobic additives, spherical micelles form because the surfactant stabilizes structures with curvatures near the optimum one (see above). For mildly hydrophobic additives, on the other hand, the wormlike-to-sphere transition can be mainly ascribed to the nonpolar molecules, which increasingly favor spherical micelles (see $x_{NP}\Delta\mu_{NP}^*$ in Figure 5c).

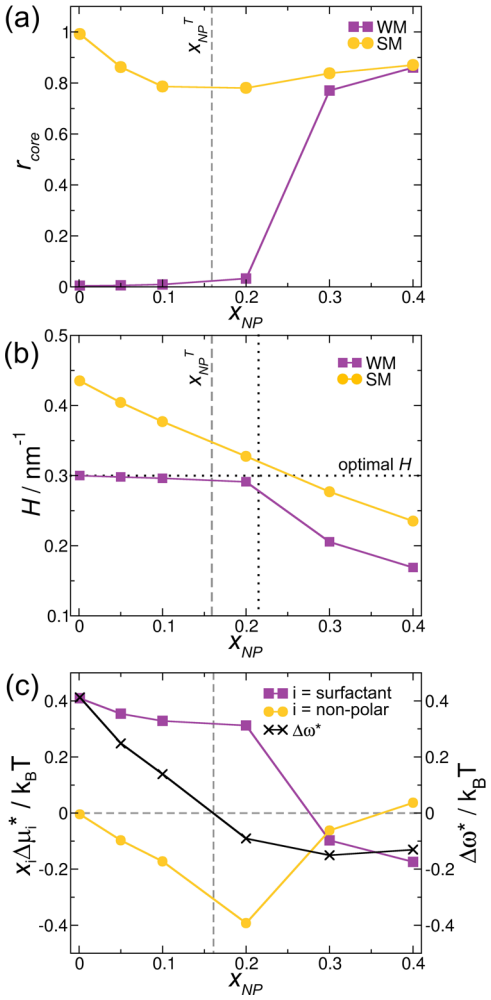

Figure 5. (a) Fraction of nonpolar molecules located at the core of the aggregates, r_{core}, as a function of their mole fraction, x_{NP}, for wormlike (purple squares) and spherical (yellow circles) micelles. (b) Mean curvature of aggregates, H, as a function of x_{NP} for wormlike (purple squares) and spherical (yellow circles) micelles. The horizontal dashed line marks the optimal curvature, and the vertical dotted line marks the x_{NP} value at which the micelle curvature is closer to the ideal curvature than that of the cylinder. (c) Change in free energy in the wormlike-to-sphere transition ($\Delta\omega^*$) and $x_i\Delta\mu_i^*$ contributions to $\Delta\omega^*$ as a function of x_{NP}. In plots (a)−(c), the gray vertical dashed line indicates the x_{NP} at the wormlike-to-sphere transition, x_{NP}^{T}. The salt concentration was fixed to 0.1 M and ϵ_{NP-NP} to 3.5 k_BT.

The large changes in the chemical potential of the nonpolar molecule as a function of x_{NP} in Figure 5c indicate that the wormlike-to-sphere transition for mildly hydrophobic additives cannot be solely rationalized in terms of the optimal curvature for the surfactant. Therefore, the effect of curvature on both the surfactant and the nonpolar additive should be taken into account. In pure-surfactant micelles, the surfactant molecules are best stabilized in a wormlike micelle with a mean curvature $H \sim 0.3$ nm^{-1}; see Figure 5b. Added nonpolar molecules can go either to the core of the aggregate or to the hydrophobic−

https://dx.doi.org/10.1021/acs.langmuir.0c03421
Langmuir 2021, 37, 3093−3103

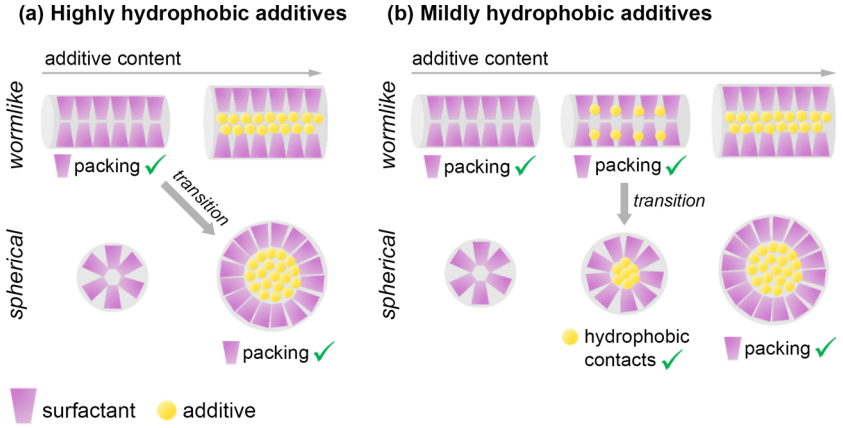

Figure 6. Schematic drawings highlighting the mechanisms behind the effect of (a) highly and (b) mildly hydrophobic additives on the morphology of the system. In the system without the additive, the surfactant packing is optimized for the wormlike micelle (see upper left drawings in (a) and (b)). In the presence of highly hydrophobic additives (a), which reside at the core of the aggregate, the curvature of the aggregates decreases as the additive content increases and the best packing is achieved by the spherical micelles (see the lower-right drawing in (a)). In the presence of mildly hydrophobic additives (b), the nonpolar molecules are located at the hydrophobic−hydrophilic interface of the wormlike micelle, which maintains the aggregate diameter and, thus, the optimal curvature for surfactant packing (see the upper-central drawing in (b)). Meanwhile, the nonpolar molecules are located at the core of spherical micelles, optimizing the hydrophobic contacts between additive molecules (see the lower-central drawing in (b)). A competition between the contribution of the chemical potential of the nonpolar and the surfactant molecules occurs, and the wormlike-to-sphere transition takes place when the latter dominates over the former. When the additive content is high (right drawings in (b)), the nonpolar molecules are located at the center of both types of aggregates, which increases their diameter and decreases their curvature. In this condition, the curvature of the spherical micelle is closest to the optimal one for the surfactant, so spheres continue to be the most stable morphology.

hydrophilic interface. The first option maximizes the hydrophobic contacts in the system, causing an increase in the size of the aggregates and hence a decrease in their mean curvature. The second option approximately maintains the size and surface curvature of the aggregates, but the number of hydrophobic contacts is suboptimal because nonpolar molecules make contact with the hydrophilic surfactant head and the solvent. In the case of spherical micelles, locating the nonpolar additive at the core is favored by both mechanisms (note that the mean curvature of the micelle is larger than the optimal one and, therefore, increasing its size stabilizes the surfactant). On the other hand, in the wormlike micelle, the maximization of the hydrophobic contacts is desirable, but the decrease in curvature resulting from locating the additive at the core is unfavorable for the surfactant, which is in an environment of optimal curvature in the absence of the additive. Therefore, in wormlike micelles, there is a competition between the stabilization of the surfactant and the nonpolar additive. As expected, for highly hydrophobic additives (results in Figure 4), the maximization of the hydrophobic contacts is the dominating effect; therefore, the nonpolar molecules are always located at the micelle core. On the contrary, for mildly hydrophobic additives, both effects are comparable. At low additive content ($x_{NP} < 0.25$), the surfactant-packing effect dominates and the nonpolar molecules are located at the hydrophobic−hydrophilic interface, while at high additive content ($x_{NP} > 0.25$), the system seeks to maximize the number of hydrophobic contacts and the nonpolar guests are located at the core of the wormlike micelle. These mechanisms explain the two regimes observed in Figure 5.

Note that the wormlike-to-sphere transition (vertical gray lines in Figure 5a−c) takes place at a mole fraction of the additive ($x_{NP}^{T} = 0.161$) smaller than that of the crossover between the two structural regimes discussed in the previous paragraph ($x_{NP} \sim 0.25$). The transition occurs when the change in free energy is zero, $\Delta\omega^* \cong x_S\Delta\mu_S^* + x_{NP}\Delta\mu_{NP}^* = 0$. Figure 5c shows that for $x_{NP} < 0.25$, the contribution of the chemical potential of the surfactant, $x_S\Delta\mu_S^*$, is positive and roughly constant with x_{NP}, while that of the nonpolar additive, $x_{NP}\Delta\mu_{NP}^*$, is negative and decreases with x_{NP}. $\Delta\omega^*$ becomes zero when the $x_{NP}\Delta\mu_{NP}^*$ and $x_S\Delta\mu_S^*$ terms compensate one another. Note that this compensation occurs before the nonpolar molecules relocate to the core of wormlike micelles, and consequently, wormlike micelles having additive molecules at their core are never an equilibrium structure in the mild hydrophobicity regime. The reason why $x_{NP}\Delta\mu_{NP}^*$ and $x_S\Delta\mu_S^*$ terms compensate is that nonpolar molecules are located at the hydrophobic−hydrophilic interface in wormlike micelles and at the core in spherical micelles. Therefore, as the additive content increases, $x_{NP}\Delta\mu_{NP}^*$ is increasingly negative (it increasingly favors the spherical shape) because the number of tail-additive hydrophobic contacts is larger in the sphere (additive in the core) than in the wormlike (additive at the hydrophobic−hydrophilic interface). Meanwhile, $x_S\Delta\mu_S^*$ is positive and constant (it constantly favors the wormlike micelles) because the curvature of wormlike micelles maintains its optimal value for surfactants as x_{NP} increases in the 0−0.2 range (see Figure 5b). In other words, the wormlike-to-sphere transition occurs when the free-energy gain of placing the nonpolar molecules at the core of the spheres (yellow lines in Figure 5c) balances the free-energy loss of changing the local packing of the surfactant in the wormlike-to-sphere transition (purple lines in Figure 5c). The proposed mechanism is schematized in Figure 6b.

The mechanism proposed in the previous paragraphs explains why the additive mole fraction at the transition increases with decreasing hydrophobicity for $\epsilon_{NP-NP} < 4.5\ k_BT$ (see Figure 2a). As the additive becomes less hydrophobic, the energy gain of forming hydrophobic contacts at the core of the spherical micelles decreases. Therefore, it is necessary to increase the amount of the additive to balance the loss in free

https://dx.doi.org/10.1021/acs.langmuir.0c03421
Langmuir 2021, 37, 3093−3103

energy that results from changing the local curvature of the surfactant molecules (see the change in the chemical potential of nonpolar molecules as a function of hydrophobicity in Figure S3 in the SI).

CONCLUSIONS

In summary, we have successfully developed a model to study the co-assembly of surfactants and additives in water−salt solutions. The model was able to reproduce several experimental trends and provided useful molecular insights into the phenomena that arise when small nonpolar molecules are encapsulated within aggregates formed by viscoelastic surfactants.

We have shown that the distribution of nonpolar molecules in the aggregates governs the mechanisms of the morphological transformations in surfactant−additive co-aggregates. We highlight next the molecular mechanisms derived from our MOLT predictions, which are schematized in Figure 6.

Highly Hydrophobic Additives. Highly hydrophobic additives, in both wormlike and spherical micelles, occupy the core of the aggregates. This organization optimizes the number of hydrophobic contacts between the nonpolar molecule and the tail of the surfactant.

For highly hydrophobic additives, the mole fraction of the additive at the transition is determined by the increase in micellar size due to the accumulation of nonpolar molecules at the core of the aggregate. As the size of the aggregates increases, the morphology shifts from cylindrical to spherical to keep the curvature of the aggregate close to the one that optimizes the packing of surfactant molecules.

Mildly Hydrophobic Additives. Mildly hydrophobic additives in wormlike micelles are located at the hydrophobic−hydrophilic interface. This organization prevents an increase in the diameter of the micelle with increasing additive content. This regime arises because keeping a constant micelle diameter stabilizes the surfactant, whose packing is optimal in the additive-free micelle.

Mildly hydrophobic additives in spherical micelles are located at the core. This strategy optimizes both the hydrophobic contacts of nonpolar molecules and the packing of the surfactant.

For mildly hydrophobic additives, the fraction of the additive at the wormlike-to-micelle transition results from a competition between the contribution to the free energy of the surfactant and the nonpolar molecules. This competition occurs because the additive is located at the hydrophobic−hydrophilic interface rather than at the core of wormlike micelles. This mechanism explains the increase in the critical amount of the additive required for the transition (x_{NP}^{T}) compared with the case of highly hydrophobic additives.

In the future, we plan to apply our model to study how the molecular structure of the surfactant and the nonpolar molecule may affect the system. In particular, we plan to consider additives and surfactants with more complex structures, for example, additives that present amphiphilic properties, which can lead to qualitatively different morphological outcomes. Furthermore, the concentration and molecular structure of the salt ions (*i.e.*, inorganic *vs* organic ions) are expected to influence the presented results. We are also interested in developing a molecular theory for surfactant self-assembly, allowing inhomogeneities in more than one spatial dimension. Such theory will allow us to study micellar shapes more complex than the ideal spherical and cylindrical morphologies considered here, for example, short wormlike micelles. These short wormlike micelles are essential to understand the morphological details of VES upon the addition of nonpolar molecules before they break into spheres.

ASSOCIATED CONTENT

Supporting Information

The Supporting Information is available free of charge at https://pubs.acs.org/doi/10.1021/acs.langmuir.0c03421.

Detailed description of the theoretical methods, size of micelles as a function of additive content, and chemical potential of an additive as a function of its hydrophobicity (PDF)

AUTHOR INFORMATION

Corresponding Author

Mario Tagliazucchi − *Departamento de Química Inorgánica, Analítica y Química Física, Facultad de Ciencias Exactas y Naturales, Universidad de Buenos Aires, Buenos Aires C1428EHA, Argentina; Instituto de Química de los Materiales, Medio Ambiente y Energía (INQUIMAE), CONICET—Universidad de Buenos Aires, Buenos Aires C1428EHA, Argentina;* orcid.org/0000-0003-4755-955X; Email: mario@qi.fcen.uba.ar; http://www.inquimae.fcen.uba.ar/softmaterials/

Authors

Gervasio Zaldivar − *Departamento de Química Inorgánica, Analítica y Química Física, Facultad de Ciencias Exactas y Naturales, Universidad de Buenos Aires, Buenos Aires C1428EHA, Argentina; Instituto de Química de los Materiales, Medio Ambiente y Energía (INQUIMAE), CONICET—Universidad de Buenos Aires, Buenos Aires C1428EHA, Argentina*

Martin Conda-Sheridan − *Department of Pharmaceutical Sciences, College of Pharmacy, University of Nebraska Medical Center, Omaha, Nebraska 68198-6125, United States;* orcid.org/0000-0002-3568-2545

Complete contact information is available at: https://pubs.acs.org/10.1021/acs.langmuir.0c03421

Author Contributions

The manuscript was written through contributions of all authors. All authors have given approval to the final version of the manuscript.

Notes

The authors declare no competing financial interest.

ACKNOWLEDGMENTS

M.T. is a fellow of CONICET. M.T. acknowledges financial support from Agencia Nacional de Promoción Científica y Tecnológica (ANPCyT) PICT 0154-2016. The authors acknowledge a CONICET-NIH Level 1 Bilateral Cooperation Grant. M.C.-S. acknowledges support from the National Science Foundation (CAREER Award # 1941731). This work was completed utilizing the Holland Computing Center of the University of Nebraska, which receives support from the Nebraska Research Initiative.

REFERENCES

(1) Dreiss, C. A.; Feng, Y. *Wormlike Micelles*; Soft Matter Series; Royal Society of Chemistry, 2017.

(2) Yang, J. Viscoelastic Wormlike Micelles and Their Applications. *Curr. Opin. Colloid Interface Sci.* **2002**, *7*, 276−281.
(3) Dreiss, C. A. Wormlike Micelles: Where Do We Stand? Recent Developments, Linear Rheology and Scattering Techniques. *Soft Matter* **2007**, *3*, 956−970.
(4) Raghavan, S. R.; Douglas, J. F. The Conundrum of Gel Formation by Molecular Nanofibers, Wormlike Micelles, and Filamentous Proteins: Gelation without Cross-Links? *Soft Matter* **2012**, *8*, 8539−8546.
(5) Rhein, L. D.; Schlossman, M.; O'Lenick, A.; Somasundaran, P. *Surfactants in Personal Care Products and Decorative Cosmetics*; CRC Press, 2006.
(6) Samuel, M. M.; Card, R. J.; Nelson, E. B.; Brown, J. E.; Vinod, P. S.; Temple, H. L.; Qu, Q.; Fu, D. K. Polymer-Free Fluid for Fracturing Applications. *SPE Drill. Completion* **1999**, *14*, 240−246.
(7) Samuel, M. M.; Dismuke, K. I.; Card, R. J.; Brown, J. E.; England, K. W. Methods of Fracturing Subterranean Formations. US6,306,800B1, Oct 23, 2001.
(8) Kefi, S.; Lee, J.; TL, P.; Sullivan, P.; Nelson, E.; AN, H.; Olsen, T.; Parlar, M.; Powers, B.; Roy, A.; Wilson, A.; Twynam, A. Expanding Applications for Viscoelastic Surfactants. *Oilfield Rev.* **2004**, *16*, 10−23.
(9) Chase, B.; Chmilowski, W.; Marcinew, R.; Mïtchell, C.; Dang, Y. Clear Fracturing Fluids for Increased Well Productivity. *Oilfield Rev.* **1997**, *09*, 20−33.
(10) Crews, J. B.; Huang, T.; Gabrysch, A. D.; Treadway, J. H.; Willingham, J. R.; Kelly, P. A.; Wood, W. R. Methods and Compositions for Fracturing Subterranean Formations. US8,188,015B2, May 29, 2012.
(11) Shibaev, A. V.; Tamm, M. V.; Molchanov, V. S.; Rogachev, A. V.; Kuklin, A. I.; Dormidontova, E. E.; Philippova, O. E. How a Viscoelastic Solution of Wormlike Micelles Transforms into a Microemulsion upon Absorption of Hydrocarbon: New Insight. *Langmuir* **2014**, *30*, 3705−3714.
(12) Hoffmann, H.; Ebert, G. Surfactants, Micelles and Fascinating Phenomena. *Angew. Chem., Int. Ed.* **1988**, *27*, 902−912.
(13) Hoffmann, H.; Ulbricht, W. Transition of Rodlike to Globular Micelles by the Solubilization of Additives. *J. Colloid Interface Sci.* **1989**, *129*, 388−405.
(14) Sato, T.; Acharya, D. P.; Kaneko, M.; Aramaki, K.; Singh, Y.; Ishitobi, M.; Kunieda, H. Oil-induced Structural Change of Wormlike Micelles in Sugar Surfactant Systems. *J. Dispersion Sci. Technol.* **2006**, *27*, 611−616.
(15) Törnblom, M.; Henriksson, U. Effect of Solubilization of Aliphatic Hydrocarbons on Size and Shape of Rodlike C16TABr Micelles Studied by 2H NMR Relaxation. *J. Phys. Chem. B* **1997**, *101*, 6028−6035.
(16) McCoy, T. M.; Valiakhmetova, A.; Pottage, M. J.; Garvey, C. J.; de Campo, L.; Rehm, C.; Kuryashov, D. A.; Tabor, R. F. Structural Evolution of Wormlike Micellar Fluids Formed by Erucyl Amidopropyl Betaine with Oil, Salts, and Surfactants. *Langmuir* **2016**, *32*, 12423−12433.
(17) Kefi, L.; Pope, S.; Nelson, H.; ez, O.; Parlar, P.; Roy, W.; Twynam, E. W. Expanding Applications for Viscoelastic Surfactants. *Oilfield Rev. 15*, 1 23.
(18) Kumar, S.; Bansal, D.; Kabir-ud-Din. Micellar Growth in the Presence of Salts and Aromatic Hydrocarbons: Influence of the Nature of the Salt. *Langmuir* **1999**, *15*, 4960−4965.
(19) Tang, X.; Zou, W.; Koenig, P. H.; McConaughy, S. D.; Weaver, M. R.; Eike, D. M.; Schmidt, M. J.; Larson, R. G. Multiscale Modeling of the Effects of Salt and Perfume Raw Materials on the Rheological Properties of Commercial Threadlike Micellar Solutions. *J. Phys. Chem. B* **2017**, *121*, 2468−2485.
(20) Lee, O.-S.; Stupp, S. I.; Schatz, G. C. Atomistic Molecular Dynamics Simulations of Peptide Amphiphile Self-Assembly into Cylindrical Nanofibers. *J. Am. Chem. Soc.* **2011**, *133*, 3677−3683.
(21) Lee, O.-S.; Cho, V.; Schatz, G. C. Modeling the Self-Assembly of Peptide Amphiphiles into Fibers Using Coarse-Grained Molecular Dynamics. *Nano Lett.* **2012**, *12*, 4907−4913.
(22) Sangwai, A. V.; Sureshkumar, R. Coarse-Grained Molecular Dynamics Simulations of the Sphere to Rod Transition in Surfactant Micelles. *Langmuir* **2011**, *27*, 6628−6638.
(23) Liu, Q.; Ji, X.; Wang, S.; Zou, W.; Li, J.; Lv, D.; Yin, B.; Yan, H.; Wei, X. Effect of Additives on Surfactant Micelle Shape Transformation: Rheology and Molecular Dynamics Studies. *J. Phys. Chem. C* **2019**, *123*, 2922−2932.
(24) Mandal, T.; Koenig, P. H.; Larson, R. G. Nonmonotonic Scission and Branching Free Energies as Functions of Hydrotrope Concentration for Charged Micelles. *Phys. Rev. Lett.* **2018**, *121*, No. 038001.
(25) Wang, H.; Tang, X.; Eike, D. M.; Larson, R. G.; Koenig, P. H. Scission Free Energies for Wormlike Surfactant Micelles: Development of a Simulation Protocol, Application, and Validation for Personal Care Formulations. *Langmuir* **2018**, *34*, 1564−1573.
(26) Cates, M. E.; Candau, S. J. Statics and Dynamics of Worm-like Surfactant Micelles. *J. Phys.: Condens. Matter* **1990**, *2*, 6869−6892.
(27) Nagarajan, R.; Ruckenstein, E. Theory of Surfactant Self-Assembly: A Predictive Molecular Thermodynamic Approach. *Langmuir* **1991**, *7*, 2934−2969.
(28) Lauw, Y.; Leermakers, F. A. M.; Cohen Stuart, M. A. Self-Consistent-Field Prediction for the Persistence Length of Wormlike Micelles of Nonionic Surfactants. *J. Phys. Chem. B* **2003**, *107*, 10912−10918.
(29) May, S.; Ben-Shaul, A. Molecular Theory of the Sphere-to-Rod Transition and the Second CMC in Aqueous Micellar Solutions. *J. Phys. Chem. B* **2001**, *105*, 630−640.
(30) Danov, K. D.; Kralchevsky, P. A.; Stoyanov, S. D.; Cook, J. L.; Stott, I. P. Analytical Modeling of Micelle Growth. 2. Molecular Thermodynamics of Mixed Aggregates and Scission Energy in Wormlike Micelles. *J. Colloid Interface Sci.* **2019**, *551*, 227−241.
(31) Danov, K. D.; Kralchevsky, P. A.; Stoyanov, S. D.; Cook, J. L.; Stott, I. P. Analytical Modeling of Micelle Growth. 3. Electrostatic Free Energy of Ionic Wormlike Micelles − Effects of Activity Coefficients and Spatially Confined Electric Double Layers. *J. Colloid Interface Sci.* **2021**, *581*, 262−275.
(32) Chen, C.; Wang, S.; Grady, B. P.; Harwell, J. H.; Shiau, B.-J. Oil-Induced Viscoelasticity in Micellar Solutions of Alkoxy Sulfate. *Langmuir* **2019**, *35*, 12168−12179.
(33) Choi, F.; Chen, R.; Acosta, E. J. Predicting the Effect of Additives on Wormlike Micelle and Liquid Crystal Formation and Rheology with Phase Inversion Phenomena. *J. Colloid Interface Sci.* **2020**, *564*, 216−229.
(34) Szleifer, I.; Carignano, M. A. Tethered Polymer Layers. *Advances in Chemical Physics*; John Wiley & Sons, Inc., 1996; Vol. *96*, pp 165−260.
(35) Guerin, C. B. E.; Szleifer, I. Self-Assembly of Model Nonionic Amphiphilic Molecules. *Langmuir* **1999**, *15*, 7901−7911.
(36) Nap, R.; Gong, P.; Szleifer, I. Weak Polyelectrolytes Tethered to Surfaces: Effect of Geometry, Acid−Base Equilibrium and Electrical Permittivity. *J. Polym. Sci., Part B: Polym. Phys.* **2006**, *44*, 2638−2662.
(37) Zaldivar, G.; Samad, M. B.; Conda-Sheridan, M.; Tagliazucchi, M. Self-Assembly of Model Short Triblock Amphiphiles in Dilute Solution. *Soft Matter* **2018**, *14*, 3171−3181.
(38) Zaldivar, G.; Vemulapalli, S.; Udumula, V.; Conda-Sheridan, M.; Tagliazucchi, M. Self-Assembled Nanostructures of Peptide Amphiphiles: Charge Regulation by Size Regulation. *J. Phys. Chem. C* **2019**, *123*, 17606−17615.
(39) Wan, T.; Wang, D.; Hu, J.; Zhou, Z.; Zhang, H.; Bu, D. Rheological Behavior of Viscoelastic Wormlike Micelles in CTAB/SSS/H2O Systems. *J. Dispersion Sci. Technol.* **2014**, *35*, 7−13.
(40) Kuperkar, K.; Abezgauz, L.; Danino, D.; Verma, G.; Hassan, P. A.; Aswal, V. K.; Varade, D.; Bahadur, P. Viscoelastic Micellar Water/CTAB/NaNO3 Solutions: Rheology, SANS and Cryo-TEM Analysis. *J. Colloid Interface Sci.* **2008**, *323*, 403−409.
(41) Israelachvili, J. N.; Mitchell, D. J.; Ninham, B. W. Theory of Self-Assembly of Hydrocarbon Amphiphiles into Micelles and Bilayers. *J. Chem. Soc., Faraday Trans. 2* **1976**, *72*, 1525−1568.

https://dx.doi.org/10.1021/acs.langmuir.0c03421
Langmuir 2021, 37, 3093−3103

(42) Rubinstein, M.; Colby, R. H. *Polymer Physics*; Oxford University Press: New York, 2003; Vol. *23*.
(43) Flory, P.; Volkenstein, M. *Statistical Mechanics of Chain Molecules*; Wiley Online Library, 1969.
(44) Marrink, S. J.; Risselada, H. J.; Yefimov, S.; Tieleman, D. P.; de Vries, A. H. The MARTINI Force Field: Coarse Grained Model for Biomolecular Simulations. *J. Phys. Chem. B* **2007**, *111*, 7812−7824.
(45) Illa-Tuset, S.; Malaspina, D. C.; Faraudo, J. Coarse-Grained Molecular Dynamics Simulation of the Interface Behaviour and Self-Assembly of CTAB Cationic Surfactants. *Phys. Chem. Chem. Phys.* **2018**, *20*, 26422−26430.
(46) Grunewald, F.; Rossi, G.; de Vries, A. H.; Marrink, S. J.; Monticelli, L. Transferable MARTINI Model of Poly (Ethylene Oxide). *J. Phys. Chem. B* **2018**, *122*, 7436−7449.
(47) Sangster, J. Octanol-Water Partition Coefficients of Simple Organic Compounds. *J. Phys. Chem. Ref. Data* **1989**, *18*, 1111−1229.

https://dx.doi.org/10.1021/acs.langmuir.0c03421
Langmuir 2021, 37, 3093−3103